

See discussions, stats, and author profiles for this publication at: <https://www.researchgate.net/publication/263652182>

# Enhanced Crystallinity in Organic-Inorganic Lead Halide Perovskites on Mesoporous TiO<sub>2</sub> via Disorder-Order Phase Transition

ARTICLE *in* CHEMISTRY OF MATERIALS · JULY 2014

Impact Factor: 8.35 · DOI: 10.1021/cm501541p

---

CITATIONS

33

READS

475

## 7 AUTHORS, INCLUDING:



[Byung-wook Park](#)

Ulsan National Institute of Science and Tech...

25 PUBLICATIONS 257 CITATIONS

[SEE PROFILE](#)



[Bertrand Philippe](#)

Uppsala University

16 PUBLICATIONS 252 CITATIONS

[SEE PROFILE](#)



[Anders Hagfeldt](#)

École Polytechnique Fédérale de Lausanne

391 PUBLICATIONS 31,907 CITATIONS

[SEE PROFILE](#)



[Gerrit Boschloo](#)

Uppsala University

197 PUBLICATIONS 14,077 CITATIONS

[SEE PROFILE](#)

# Enhanced Crystallinity in Organic–Inorganic Lead Halide Perovskites on Mesoporous $\text{TiO}_2$ via Disorder–Order Phase Transition

Byung-wook Park,<sup>†</sup> Bertrand Philippe,<sup>§</sup> Torbjörn Gustafsson,<sup>‡</sup> Kári Sveinbjörnsson,<sup>†</sup> Anders Hagfeldt,<sup>†,⊥</sup> Erik M. J. Johansson,<sup>\*,†</sup> and Gerrit Boschloo<sup>\*,†</sup>

<sup>†</sup>Uppsala University, Department of Chemistry—Ångström Laboratory, Box 523, SE 751 20 Uppsala, Sweden

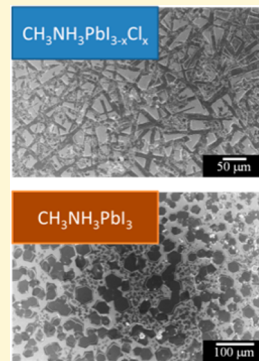
<sup>‡</sup>Uppsala University, Department of Chemistry—Ångström Laboratory, Structural Chemistry, Box 538, 751 21 Uppsala, Sweden

<sup>§</sup>Uppsala University, Department of Physics and Astronomy, Molecular and Condensed Matter Physics, Box 516, SE 751 20 Uppsala, Sweden

<sup>⊥</sup>School of Chemical Engineering, Sungkyunkwan University, Suwon 440-746, Korea

## Supporting Information

**ABSTRACT:** Organic–inorganic halide perovskite (OIHP) compounds are very interesting materials for device application in, for example, solar cells, electro-optics, and electronic circuits. In this report, we investigated OIHPs reported as  $\text{CH}_3\text{NH}_3\text{PbI}_{3-x}\text{Cl}_x$  ( $\text{MAPbI}_{3-x}\text{Cl}_x$ ) and  $\text{CH}_3\text{NH}_3\text{PbI}_3$  ( $\text{MAPbI}_3$ ) prepared from solution on mesoporous  $\text{TiO}_2$ /glass substrates. A long-term conversion from disordered to more crystalline OIHPs was observed for both types of samples from XRD patterns over 5 weeks. The conversion rate to more crystalline OIHPs could be increased by increasing the temperature of the sample. SEM analyses of the two types of OIHPs show remarkably different surface microstructures. The X-ray diffractograms suggest that both samples are dominated by the similar crystal structure, although the preferential orientation for the crystal structure is different. Moreover, the results suggest that the material reported as  $\text{MAPbI}_{3-x}\text{Cl}_x$  is a combination of  $\text{MAPbI}_3$  and  $\text{MAPbCl}_3$ . The crystal structure and exact nature of the material is important for the understanding and optimization of devices, and the possibility for enhanced crystallinity of the OIHPs shown in this report will therefore be important for further improvement and understanding of the devices.



## 1. INTRODUCTION

Organic–inorganic metal halide perovskites (OIHPs) are interesting materials for use in many different applications. For example, OIHP compounds for field-effect transistors and optoelectronic devices have been developed, and different preparation methods have been used, for example, deposition from a metal–organic precursor by spin-coating.<sup>1a–c</sup> Furthermore, organic–inorganic metal halide perovskites (OIHPs) have appeared as interesting materials in the field of solar cell research.

Recently,  $\text{CH}_3\text{NH}_3\text{PbI}_3$  ( $\text{MAPbI}_3$ ) and  $\text{CH}_3\text{NH}_3\text{PbI}_{3-x}\text{Cl}_x$  ( $\text{MAPbI}_{3-x}\text{Cl}_x$ ) OIHPs have been used for solid state organic/inorganic heterojunction thin film photovoltaic (PV) cells with very high power conversion efficiency.<sup>2–4</sup> The first concept of OIHP based PV cell was published by Miyasaka et al. in 2009 where the OIHPs methylamine hydrogen lead tri-iodide ( $\text{MAPbI}_3$ ) and methylamine hydrogen lead tribromide ( $\text{MAPbBr}_3$ ) were used as sensitizers.<sup>2a</sup> They recorded power conversion efficiencies (PCEs) of 3.8% ( $\text{MAPbI}_3$ ) and 3.1% ( $\text{MAPbBr}_3$ ) with a liquid redox electrolyte. An improved efficiency (6.5%) of the  $\text{MAPbI}_3$  sensitized PV cell with liquid electrolyte was reported by Nam-Gyu Park et al. in 2011.<sup>2b</sup> Replacing the liquid redox electrolyte with a solid state hole transport material, spiro-OMeTAD, resulted in a significant improvement of the efficiency, and a PCE of around 9% was

reported using a submicron mesoporous  $\text{TiO}_2$  (ms- $\text{TiO}_2$ ) based  $\text{CH}_3\text{NH}_3\text{PbI}_3$ /spiro-MeOTAD system.<sup>2c</sup> Recent publications have shown even higher PCE for systems based on  $\text{MAPbI}_3$  or  $\text{MAPbI}_{3-x}\text{Cl}_x$  OIHPs,<sup>2,3</sup> and the possibility to remove the organic hole conductor has also been shown, which simplifies the structure of the solar cell even further.<sup>2d</sup> The long-term stability is still an important issue that needs to be studied and addressed.<sup>2,3</sup> The OIHPs have been reported to demonstrate high stability in dry air condition or nitrogen gas atmosphere.<sup>2c</sup> However, a long-term decay of the efficiency in solar cell performance may be caused by high humidity or UV light,<sup>3c</sup> and the aging of the OIHPs is not known in detail.

In this work, we investigate the crystalline structure of the most efficient solar cell OIHP materials reported as  $\text{CH}_3\text{NH}_3\text{PbI}_3$  ( $\text{MAPbI}_3$ ) and  $\text{CH}_3\text{NH}_3\text{PbI}_{3-x}\text{Cl}_x$  ( $\text{MAPbI}_{3-x}\text{Cl}_x$ ) and how it changes over time. Specifically, we investigate these materials prepared from solution in combination with the typical ms- $\text{TiO}_2$  structure that is used in solar cells.

Received: April 29, 2014

Revised: July 4, 2014

## 2. EXPERIMENTAL DETAIL

**2.1. Sample Fabrication.** A 1.5 M  $\text{CH}_3\text{NH}_3\text{PbI}_3$  perovskite precursor solution was formed from an equimolar mixture of  $\text{CH}_3\text{NH}_3\text{I}$  and  $\text{PbI}_2$  in dimethylformamide (DMF)/dimethyl sulfoxide (DMSO) solvent mixture (7/3 by volume). First, the metal halide compounds were completely dissolved in the solvent mixture on a hot plate at 70–80 °C for few hours, and then  $\text{CH}_3\text{NH}_3\text{I}$  was added and a homogeneous, yellow colored solution was obtained after 3–48 h.  $\text{CH}_3\text{NH}_3\text{I}$  was synthesized as described in ref 2c.  $\text{CH}_3\text{NH}_3\text{Cl}$  was synthesized in a similar fashion.  $\text{CH}_3\text{NH}_3\text{PbI}_{3-x}\text{Cl}_x$  perovskite was formed in a ratio of 3:1 of  $\text{CH}_3\text{NH}_3\text{I}$  (4.5 M) and  $\text{PbCl}_2$  (1.5 M) in the same solvent.<sup>3d</sup>  $\text{CH}_3\text{NH}_3\text{PbI}_3$  perovskite of 1.5 M ratio concentration was also formed in equimolar ratio of  $\text{CH}_3\text{NH}_3\text{I}$  and  $\text{PbI}_2$ .<sup>2c,3d</sup>  $\text{CH}_3\text{NH}_3\text{PbCl}_3$  perovskite of 1.5 M ratio concentration was prepared as a precursor in an equimolar ratio of  $\text{CH}_3\text{NH}_3\text{Cl}$  and  $\text{PbCl}_2$  in DMSO. DMSO can be used for better solubility of metal halide compounds. The precursors are filtered by PVDF syringe filter (Whatman, 0.45 mm pore).  $\text{TiO}_2$  nanoparticles were deposited on microscope glass by spin-coating method at 3500 rpm for 30 s. The  $\text{TiO}_2$  paste was prepared by diluting Dyesol paste (18NR-T, 100% anatase, particle size ca. 20 nm) with ethanol in a 1:3 weight ratio. The  $\text{TiO}_2$  nanoparticle coated microscope glass was annealed onto a hot plate at 550 °C for 30 min. The film thickness was approximately 650 nm ( $\pm 80$  nm) as determined using a Dektak3 profiler (see Supporting Information Figure S7 cross-sectional SEM image). The organic–inorganic lead halide perovskite precursor solutions were coated onto  $\text{TiO}_2$ /glass substrate by spin-coating method at 1500 rpm for 30 s, followed by annealing on a hot plate at 140 °C ( $\text{CH}_3\text{NH}_3\text{PbI}_{3-x}\text{Cl}_x$ ) and 120 °C ( $\text{CH}_3\text{NH}_3\text{PbI}_3$ ) for 30 min in dry air box (relative humidity less than 10%). Finally, samples were dried under vacuum conditions of  $5 \times 10^{-5}$  torr for 1 h in order to remove solvents from the perovskite layer completely.

**2.2. Crystallographic Properties.** The perovskites deposited on  $\text{TiO}_2$ /glass substrate were investigated for crystallographic properties using X-ray diffraction (XRD) with a Siemens D5000 diffractometer using Cu K $\alpha$  radiation. The Diffrac plus XRD commander program was used to control the instrument. The instrument was set in “detector scan” mode, and acquisition was done for every 0.02° increment over the Bragg angle range of 10–60°. Changes in the X-ray intensity of the instrument were corrected for by measuring one ms- $\text{TiO}_2$ /glass sample before measuring perovskite samples and subsequent correction of counts. Samples were precisely positioned so that always the same area was probed. The 4 h measurement was performed at room temperature in air with a relative humidity between 30% and 50%. XRD patterns of  $\text{PbCl}_2$ ,  $\text{CH}_3\text{NH}_3\text{I}$ , and  $\text{CH}_3\text{NH}_3\text{Cl}$  are given in Figure S6 in Supporting Information.

**2.3. UV–Vis Spectra.** UV–visible–NIR absorption spectra were recorded using a Cary 5000 UV–vis–NIR spectrophotometer (VARIAN, Photometric accuracy is <0.00025 Abs., Photometric range is 8 Abs.). The microscope glass substrate signal was used as reference background.

## 3. RESULTS AND DISCUSSION

The  $\text{MAPbI}_3$  and  $\text{MAPbI}_{3-x}\text{Cl}_x$  precursor solutions were prepared by mixing  $\text{CH}_3\text{NH}_3\text{I}$  and  $\text{PbI}_2$  or  $\text{PbCl}_2$  in a mixture of DMF (*N,N*-dimethylformamide) and DMSO (dimethyl sulfoxide). The solutions were heated onto hot plate at 70–80 °C for a few hours until the compounds were completely dissolved. The OIHP precursors were coated onto  $\text{TiO}_2$ /glass substrates by spin-coating, followed by annealing them on a hot-plate in a dry air box (relative humidity less than 10%) and drying in vacuum for 1 h. Crystallographic properties of the resulting OIHPs on ms- $\text{TiO}_2$ /glass substrates were investigated with X-ray diffraction (XRD), morphology by scanning electron microscopy, and optical properties by UV–vis spectroscopy.

X-ray diffractograms for two types of samples are shown in Figure 1 with  $\text{MAPbI}_{3-x}\text{Cl}_x$  (on ms- $\text{TiO}_2$ ) in the left panel and

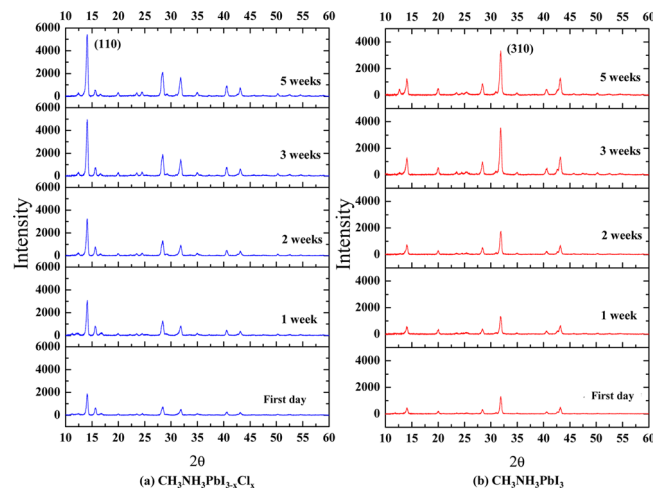


**Figure 1.** X-ray diffractograms for (a)  $\text{MAPbI}_{3-x}\text{Cl}_x$  (on mesostructured  $\text{TiO}_2$ ) and (b)  $\text{MAPbI}_3$  (on mesostructured  $\text{TiO}_2$ ) and the changes over time at a temperature of about 300 K. The ms- $\text{TiO}_2$  background is subtracted.

$\text{MAPbI}_3$  (on ms- $\text{TiO}_2$ ) in the right panel. The samples were measured during 5 weeks to study changes in crystallinity. The samples were kept in Ar gas atmosphere at room temperature between the measurements to avoid reaction with air atmosphere.<sup>2f,6</sup>

The X-ray diffractograms measured immediately after preparation of the samples were in agreement with spectra previously reported for these materials in the literature.<sup>1g,2d,e,3a,b,4a</sup> The intensities of most X-ray diffractogram peaks in Figure 1 increase with time after preparation of the samples. This is observed for both OIHP type, and it can be correlated to an increase of the crystallinity of the samples during this period.

Comparing the X-ray diffractogram of the  $\text{MAPbI}_3$  on the ms- $\text{TiO}_2$  substrate in Figure 1 to that of powdered  $\text{MAPbI}_3$  published previously,<sup>7</sup> we find diffraction peaks that correspond to the tetragonal phase {110}, {220}, {310}, {224}, and {314}. We observe, however, that in our ms- $\text{TiO}_2$  electrode sample the main diffraction peak from  $\text{MAPbI}_3$  is {310}, while it is {110} orientation in the powder sample. These results indicate that there is a preferential orientation of the crystals in the ms- $\text{TiO}_2$  structure used in the solar cell. Unlike the solar cell, our ms- $\text{TiO}_2$  samples are on glass, rather than on a dense  $\text{TiO}_2$  layer. Considering that the area of the perovskite/glass interface is about 100 times smaller than the perovskite/ms- $\text{TiO}_2$  interface, we assume the glass has no significant effect on perovskite crystallinity. Other scaffold layers, such as mesoporous  $\text{Al}_2\text{O}_3$ , may affect the OIHP crystallinity in a different way than ms- $\text{TiO}_2$  (anatase). This topic lies outside the scope of this paper.

We also found that the aging time of the precursor solution had significant effects on the resulting microcrystalline structure of the deposited perovskite. XRD diffractograms and SEM micrographs are given in Figure S5 of the Supporting Information. This effect is important for structural control of the resulting perovskite films but will not be discussed further here. All films discussed here were made from fresh precursor solutions (less than 2 h old).

The powder XRD diffractogram for  $\text{MAPbI}_{3-x}\text{Cl}_x$  has not yet been reported, and it is therefore difficult to make any conclusion about the preferred crystal direction in the solar cell sample. However, in the X-ray diffractogram from this sample,

the preferential orientation is  $\{110\}$ , which indicates that the OIHP in this sample has a different preferred orientation compared to the other sample.

The Scherrer equation was used to estimate an average crystallite size from the width of the main peaks in the X-ray diffractograms.<sup>8a,b</sup> Crystal sizes of approximately 20–25 nm were obtained, which were rather constant during the aging period of 5 weeks (see Figure s1 of the Supporting Information). The result is reasonable since the pore size in the mesoporous  $\text{TiO}_2$  layer is around 20–25 nm, which may limit the growth of larger OIHP crystals. Interestingly, the intensity of the XRD peaks increased during aging. This suggests that more crystallites are formed. Possibly, there is some growth of crystallites and simultaneous formation of new small crystallites, overall yielding a nearly unchanged broadening in the X-ray diffractograms. Recent results using X-ray scattering on  $\text{MAPbI}_3$  in ms- $\text{TiO}_2$  suggest that only 30% of the  $\text{MAPbI}_3$  is crystalline and 70% is disordered or amorphous phase.<sup>9</sup> Our results are in qualitative agreement with this report and suggest that new crystals of OIHPs are formed from the less crystalline regions of the material.

Figure 2 shows SEM images of the surface of the two samples  $\text{MAPbI}_{3-x}\text{Cl}_x$  (on ms- $\text{TiO}_2$ ) and  $\text{MAPbI}_3$  (on ms- $\text{TiO}_2$ ). Large

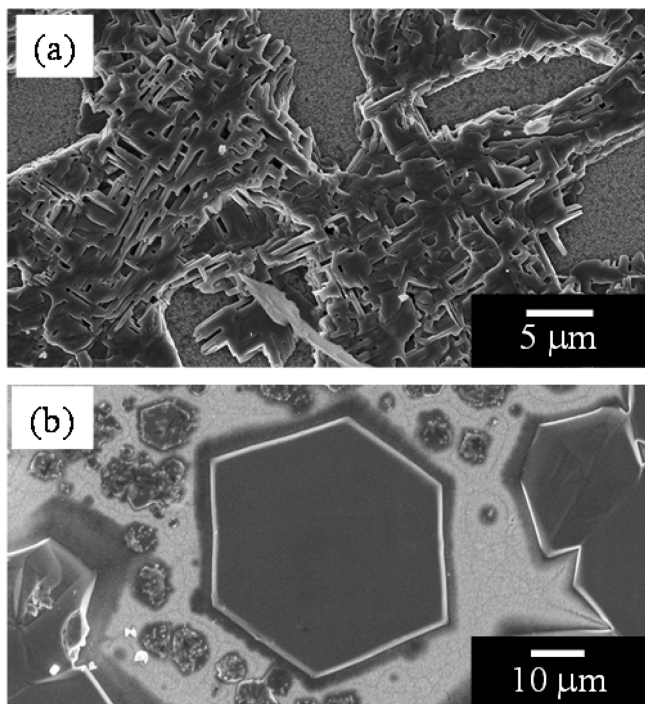


**Figure 2.** (a) SEM images of the surface structure of  $\text{MAPbI}_{3-x}\text{Cl}_x$  (on mesostructured  $\text{TiO}_2$ ) and (b)  $\text{MAPbI}_3$  (on mesostructured  $\text{TiO}_2$ ). Lower magnification images are presented in Figure s8 of the Supporting Information.

crystals are formed on top of the mesoporous films and cover about 50% of the mesoporous film. A clear difference is observed between the samples. In the  $\text{MAPbI}_{3-x}\text{Cl}_x$  sample cubic microparticles in connection with each other are observed. In the  $\text{MAPbI}_3$  sample hexagonal structures are observed, in agreement with previous work.<sup>2g</sup> There is a very clear difference in the surface texture of the OIHPs, which probably is related to the difference in the preferred crystalline direction from the XRD results shown above.

Upon magnifications of parts of the X-ray diffractograms, extra features are found that do not correspond to the expected OIHP, see Figure 3 a and c. These X-ray diffractograms are

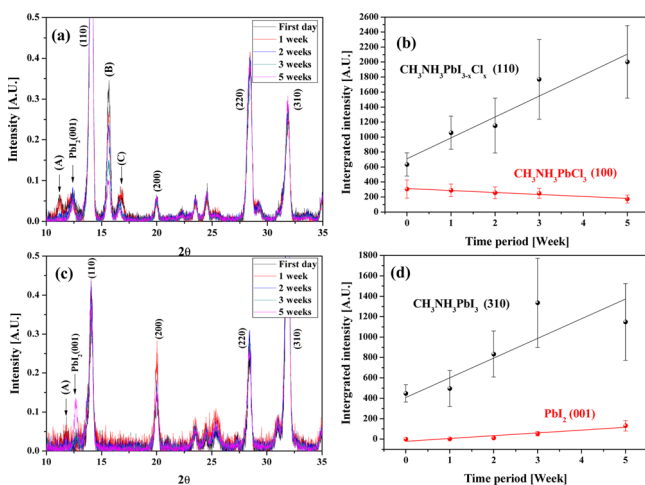


**Figure 3.** Magnifications of X-ray diffractograms from Figure s-3 (A-1) and (B-1) for samples (a)  $\text{MAPbI}_{3-x}\text{Cl}_x$  onto ms- $\text{TiO}_2$  and (c)  $\text{MAPbI}_3$  onto ms- $\text{TiO}_2$  and the changes over time. Integrated intensities from both preferential orientation peaks in the XRD spectra of Figure 1a and b for the  $\text{MAPbI}_{3-x}\text{Cl}_x$  in ms- $\text{TiO}_2$  and  $\text{MAPbI}_3$  on ms- $\text{TiO}_2$  and the changes over time.

normalized at their main diffraction peak. In the X-ray diffractograms of both samples, we observe a peak around  $2\theta = 12.5$ , which we assign to  $\text{PbI}_2$ .<sup>1g,2e</sup> In the X-ray diffractogram for the  $\text{MAPbI}_{3-x}\text{Cl}_x$  sample, we also observe a peak (B) at  $2\theta = 15.5$ . This peak can be attributed to  $\text{MAPbCl}_3$  by comparison to the pure cubic crystalline phase of  $\text{MAPbCl}_3$  shown in Figure 4 and in previous work on  $\text{MAPbCl}_3$ .<sup>10–12</sup> In the preparation of the  $\text{MAPbI}_{3-x}\text{Cl}_x$  material the results therefore suggest that some  $\text{MAPbCl}_3$  crystallites are formed. In Figure 3 a two very small peaks (A) and (C) are noted, which decrease with time. The origin of these small peaks is still unknown.

Figure 3 b and d shows the change of intensity of selected XRD peaks upon aging. As stated before, the main peaks increase with aging, due to formation of more OIHP crystallites. The signal assigned to  $\text{MAPbCl}_3$  decreases with time, which suggests that the combination of the two OIHPs is not stable. In the  $\text{MAPbI}_3$  sample the  $\text{PbI}_2$  peak increases with time, while it remains unchanged in the  $\text{MAPbI}_{3-x}\text{Cl}_x$  sample (see Figure s3 in the Supporting Information).

We prepared  $\text{MAPbI}_{3-x}\text{Cl}_x$  in ms- $\text{TiO}_2$  with different concentration of the precursors MAI and  $\text{PbCl}_2$ . Sample no. 1 in Figure 4a was prepared from  $\text{MACl}$  and  $\text{PbCl}_2$  (1:1 molar ratio) and contained pure  $\text{MAPbCl}_3$ , in good agreement with the literature.<sup>11</sup> The peak in XRD at  $2\theta = 15.5$ , assigned to the cubic  $\text{MAPbCl}_3$ ,<sup>11</sup> is very intense when the sample was prepared from similar molar ratios of  $\text{PbCl}_2$  and MAI, see Figure 4a. When the concentration of MAI is increased this peak is weaker, and when increasing the molar ratio of MAI compared to  $\text{PbCl}_2$  to about 3, the peak assigned to  $\text{MAPbCl}_3$  perovskite is minimized.

Formation of  $\text{MAPbCl}_3$  perovskite is the explanation for the difference in molar ratios of the lead salt and the MAI used in preparation of efficient solar cells based on the two materials  $\text{MAPbI}_{3-x}\text{Cl}_x$  and  $\text{MAPbI}_3$  used in previous reports.<sup>2,4</sup> The most efficient solar cells based on the material  $\text{MAPbI}_{3-x}\text{Cl}_x$  are

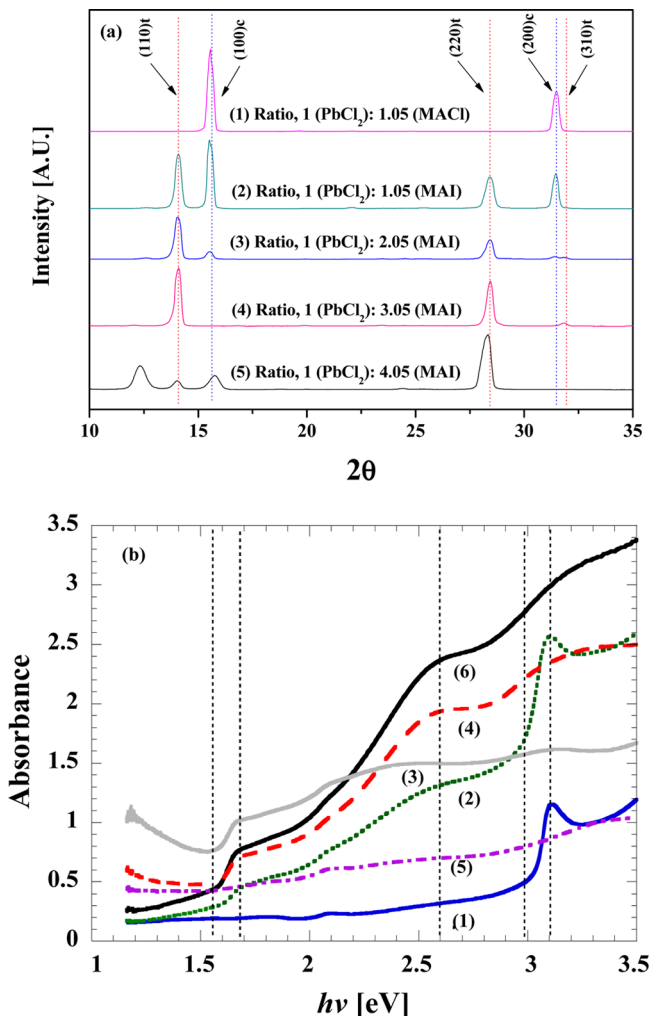


**Figure 4.** (a) X-ray diffractograms for samples  $\text{MAPbI}_{3-x}\text{Cl}_x$  in ms-TiO<sub>2</sub> prepared with different concentration of precursors, as indicated in the figure and the X-ray diffractogram of pure  $\text{MAPbCl}_3$  in ms-TiO<sub>2</sub>. (b) UV-vis spectra of the samples with different concentrations of the precursors.

made with the molar ratio 1:3 for  $\text{PbCl}_2$  and MAI, which corresponds to the composition with the lowest amount of crystalline  $\text{MAPbCl}_3$  perovskite in the samples. Interestingly, for the molar ratio 1:4 for  $\text{PbCl}_2$  and MAI, a different crystalline phase appears to be formed as the {110} tetragonal peak decreases, possibly a two-dimensional OIHP. For the  $\text{MAPbI}_3$  sample we do not observe any other OIHPs in the sample, and the molar ratio 1:1 gives the correct  $\text{MAPbI}_3$  OIHP.

Recent results on elemental analysis of  $\text{MAPbI}_{3-x}\text{Cl}_x$  based solar cells demonstrate that the amount of chloride in the material is very small, on the order of less than 4%.<sup>4b,13</sup> Our results therefore suggest that the chloride is included in small amounts of  $\text{MAPbCl}_3$  OIHP in the sample and that the main part of the perovskite is actually  $\text{MAPbI}_3$  also in the  $\text{MAPbI}_{3-x}\text{Cl}_x$  material.

Absorption spectra of the materials with different concentration of the precursors are shown in Figure 4b. The absorbtion spectrum of the  $\text{MAPbCl}_3$  sample (no. 1) shows low absorbtion in the visible region, an absorbtion onset at about 3.0 eV in good agreement with the bandgap of  $\text{MAPbCl}_3$  reported previously.<sup>14</sup> There is a characteristic excitonic absorbtion peak at 3.1 eV. For the sample no. 2 (( $\text{PbCl}_2$ ):

(MAI) = 1:1.05), a similar sharp peak is observed around 400 nm, which agrees with the suggestion that there is a certain amount of  $\text{MAPbCl}_3$  in this sample. This film has a broader absorbtion spectrum stretching over 750 nm, similar to that of the pure  $\text{MAPbI}_3$  sample (no. 6). The results from the absorbtion spectra therefore agree with a combination of crystalline  $\text{MAPbCl}_3$  and  $\text{MAPbI}_3$  in this sample, in agreement with XRD results above. For sample no. 3, ( $\text{PbCl}_2$ ):(MAI) = 1:2.05, the spectrum is rather different and there is no large peak observed around 400 nm. This suggests that the contribution from the  $\text{MAPbCl}_3$  in the absorbtion spectrum is small in this sample, which agrees with the X-ray diffractograms. For the 1 ( $\text{PbCl}_2$ ):3.05 (MAI) sample (no. 4), the shape of the absorbtion spectrum is rather similar to the absorbtion spectrum of the  $\text{MAPbI}_3$  sample. This also agrees with the suggestion above that the  $\text{MAPbCl}_3$  contribution is minimized with this molar ratio of the precursors and the sample contains mainly  $\text{MAPbI}_3$ . The absorbtion onset  $\text{MAPbCl}_3$  containing samples are at about 1.55 eV, corresponding to the bandgap and in agreement with literature.<sup>3a</sup> There are shoulders at 1.7 and 2.6 eV. Sample 5 has an unpronounced absorbtion spectrum that does not give evidence for light absorbtion by either  $\text{MAPbI}_3$  or  $\text{MAPbCl}_3$ . It should be noted that the fraction of disordered material in all samples is large and can affect the absorbtion spectrum. This may explain the significant light absorbtion at energies smaller than the bandgap of  $\text{MAPbI}_3$ . The UV-vis study was done on fresh samples, and the effect of aging was not investigated in this study.

Finally, we investigated the effect of heating OIHPs on ms-TiO<sub>2</sub> samples. The samples were exposed to air under the humidity 30%–50% for 12 h on the first day. After 1 day, the samples were kept in an Ar atmosphere and only exposed to air during the XRD measurements for 4 h each. Samples kept at 343 and 293 K in Ar gas atmosphere were compared by XRD analysis, see Figure 5. Because exposure to air during the 4 h XRD measurements can have a significant effect on the samples, two series as samples were measured. One series of the samples was measured three times during the 10 day test

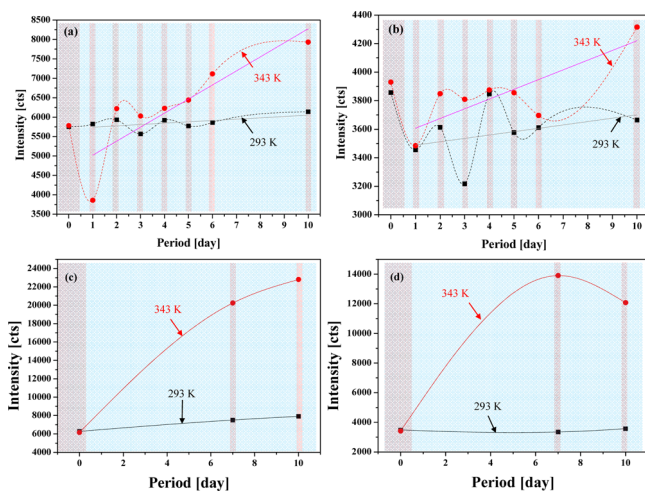


**Figure 5.** Temperature dependence of the main peak in the X-ray diffractograms for (a)  $\text{MAPbI}_{3-x}\text{Cl}_x$  and (b)  $\text{MAPbI}_3$  for measurements every day and (c)  $\text{MAPbI}_{3-x}\text{Cl}_x$  and (d)  $\text{MAPbI}_3$  for fewer measurements during the same time period. Tinted areas indicate exposure to air at room temperature.

period. At 343 K the XRD intensity of the main peak increased significantly during the 10 day period. For the samples kept at 293 K, on the other hand, the intensities were rather constant. We can therefore conclude that heating the sample has a significant effect on the enhanced crystallization. For the samples more that were more exposed to air during the 10 day period (Figure 5a, b), there was a much slower increase of crystallization compared to the samples that were kept longer in argon (Figure 5b, c). Keeping the samples in inert atmosphere seems to promote formation of more crystalline material, while exposure to ambient air suppresses this effect. Furthermore, both OIHPs show the same XRD pattern after heating the samples and do not change to another crystalline phase during the heat treatment, which is important for the stability of the OIHPs (see Table s1 and Figure s6 in the Supporting Information).

It is important to determine the ratio between the amount of crystalline material and disordered material in the samples. Above we concluded that the disordered material is transformed to more crystalline material, which is a rather slow process at room temperature. From the intensity of the main diffraction peak in the X-ray diffractograms, we can compare how the amounts of crystalline material change in the material. If we assume that after the 10-day heat treatment at 343 K most of the disordered material is transformed to crystalline material, we can estimate the ratio between the crystalline material and ordered material for the samples directly after preparation to about 30% for both  $\text{MAPbI}_{3-x}\text{Cl}_x$  and  $\text{MAPbI}_3$ . These results agree with the result from analysis of X-ray scattering of  $\text{MAPbI}_3$  in ms-TiO<sub>2</sub> where only 30% of the  $\text{MAPbI}_3$  was found to be crystalline and 70% disordered or amorphous phases.<sup>9</sup> We obtain similar results here and demonstrate that it is possible to increase the degree of crystallization by prolonged heat treatment in Ar gas atmosphere. This possibility for enhancing the crystallinity of the samples may be particularly important for improvement of the solar cell devices, where the crystallinity may have a large effect on charge conductivity and recombination.

In summary, we have investigated samples based on  $\text{MAPbI}_3$  and  $\text{MAPbI}_{3-x}\text{Cl}_x$  prepared by solution process in combination with ms-TiO<sub>2</sub> substrates. A slow increase in crystallinity of the OIHPs over weeks was observed in both cases, and the results suggest that disordered regions of material are changed to crystalline regions over time. A clear increase in the transition rate from disordered to crystalline material was observed when the samples were heated. Moreover, SEM analysis of the surface of the samples shows clear differences between the surface texture of the OIHPs, and the XRD results indicate different growth directions for  $\text{MAPbI}_{3-x}\text{Cl}_x$  and  $\text{MAPbI}_3$ .

The results also suggest that under the conditions used the  $\text{MAPbI}_{3-x}\text{Cl}_x$  sample consists of a combination of  $\text{MAPbI}_3$  and  $\text{MAPbCl}_3$ . The amount of crystalline  $\text{MAPbCl}_3$  is shown to be dependent on the concentration of the precursors in the solution. The increased crystallinity of the OIHPs by heating in Ar gas atmosphere may be of particular importance for developing OIHPs in electronic devices and solar cells.

## ASSOCIATED CONTENT

### Supporting Information

Detailed synthesis procedures and additional experimental data; XRD patterns and fitting; SEM images at lower magnification. This material is available free of charge via the Internet at <http://pubs.acs.org/>.

## AUTHOR INFORMATION

### Corresponding Authors

\*E-mail: erik.johansson@kemi.uu.se.

\*E-mail: gerrit.boschloo@kemi.uu.se.

### Notes

The authors declare no competing financial interest

## ACKNOWLEDGMENTS

We thank the Swedish Energy Agency, the STandUP for Energy program, the Swedish Research Council (VR), the Göran Gustafsson Foundation, and the Knut and Alice Wallenberg Foundation.

## REFERENCES

- (1) (a) Kagan, C. R.; Mitzi, D. B.; Dimitrakopoulos, C. D. *Science* **1999**, *286*, 945–947. (b) Mitzi, D. B.; Kosbar, L. L.; Murray, C. E.; Copel, M.; Afzali, A. *Nature* **2004**, *428*, 299–303. (c) Mitzi, D. B. *Chem. Mater.* **2001**, *13*, 3283–3298. (d) Mitzi, D. B.; Chondroudis, K.; Kagan, C. R. *IBM J. Res. Dev.* **2001**, *45* (1), 29–45. (e) Chondroudis, K.; Mitzi, D. B. *Chem. Mater.* **1999**, *11*, 3028–3030. (f) Koubaa, M.; Dammak, T.; Garrot, D.; Castro, M.; Codjovi, E.; Mlayah, A.; Abid, Y.; Boukheddaden, K. *J. Appl. Phys.* **2012**, *111*, 053521. (g) Liang, K.; Mitzi, D. B.; Prikas, M. T. *Chem. Mater.* **1998**, *10*, 403–411.
- (2) (a) Kojima, A.; Teshima, K.; Shirai, Y.; Miyasaka, T. *J. Am. Chem. Soc.* **2009**, *131*, 6050–6051. (b) Im, J.-H.; Lee, C.-R.; Lee, J.-W.; Park, S.-W.; Park, N.-G. *Nanoscale* **2011**, *3*, 4088–4093. (c) Kim, H.-S.; Lee, C.-R.; Im, J.-H.; Lee, K.-B.; Moehl, T.; Marchioro, A.; Moon, S.-J.; Humphry-Baker, R.; Yum, J.-H.; Moser, J. E.; Grätzel, M.; Park, N.-G. *Sci. Rep.* **2012**, *2*, 591. (d) Laban, W. A.; Etgar, L. *Energy Environ. Sci.* **2013**, *6*, 3249–3253. (e) Burschka, J.; Pellet, N.; Moon, S.-J.; Humphry-Baker, R.; Gao, P.; Nazeeruddin, M. K.; Grätzel, M. *Nature* **2013**, *499*, 316–319. (f) Noh, J. H.; Im, S. H.; Heo, J. H.; Mandal, T. N.; Seok, S. I. *Nano Lett.* **2013**, *13*, 1764–1769. (g) Heo, J. H.; Im, S. H.; Noh, J. H.; Mandal, T. N.; Lim, C.-S.; Chang, J. A.; Lee, Y. H.; Kim, H.-j.; Sarkar, A.; Nazeeruddin, M. K.; Grätzel, M.; Seok, S. I. *Nat. Photonics* **2013**, *7*, 486–491. (h) Im, J.-H.; Chung, J.; Kim, S.-J.; Park, N.-G. *Nanoscale Res. Lett.* **2012**, *7*, 353.
- (3) (a) Lee, M. M.; Teuscher, J.; Miyasaka, T.; Murakami, T. N.; Snaith, H. J. *Science* **2012**, *338*, 643–647. (b) Liu, M.; Johnston, M. B.; Snaith, H. J. *Nat. Commun.* **2013**, *5*, 1, 395–399. (c) Leijtens, T.; Eperon, G. E.; Pathak, S.; Abate, A.; Lee, M. M.; Snaith, H. J. *Nat. Commun.* **2013**, *4*, No. 2885, DOI: 10.1038/ncomms3885. (d) Stranks, S. D.; Eperon, G. E.; Grancini, G.; Menelaou, C.; Alcocer, M. J. P.; Leijtens, T.; Herz, L. M.; Petrozza, A.; Snaith, H. J. *Science* **2013**, *342*, 341–344. (e) Eperon, G. E.; Stranks, S. D.; Menelaou, C.; Johnston, M. B.; Herz, L. M.; Snaith, H. J. *Energy Environ. Sci.* **2014**, *7*, 982–988. (f) Snaith H.; Lee M. *Optoelectronic device comprising perovskites*. WO2013171520 A1, 2013.
- (4) (a) Chen, Q.; Zhou, H.; Hong, Z.; Luo, S.; Duan, H.-S.; Wang, H.-H.; Liu, Y.; Li, G.; Yang, Y. *J. Am. Chem. Soc.* **2014**, *136* (2), 622–625. (b) You, J.; Hong, Z.; Yang (Michael), Y.; Chen, Q.; Cai, M.; Song, T.-B.; Chen, C.-C.; Lu, S.; Liu, Y.; Zhou, H.; Yang, Y. *ACS Nano* **2014**, *8*, 1674–1680.
- (5) (a) Srodon, J.; Drits, V. A.; McCarty, D. K.; Hsieh, J. C. C.; Eberl, D. D. *Clays Clay Miner.* **2001**, *49* (6), 514–528. (b) Chung, F. H. *J. Appl. Crystallogr.* **1974**, *7*, 519–525a.
- (6) Mulliken, R. S. *J. Phys. Chem.* **1952**, *56* (7), 801–822.
- (7) Baikie, T.; Fang, Y.; Kadro, J. M.; Schreyer, M.; Wei, F.; Mhaisalkar, S. G.; Graetzel, M.; White, T. J. *J. Mater. Chem. A* **2013**, *1*, 5628–5641.
- (8) (a) Cullity, B. D. *Elements of X-ray Diffraction*; Addison-Wesley: London, 1959; p 99. (b) Li, L.; Fang, L.; Chen, X. M.; Liu, J.; Yang, F. F.; Li, Q. J.; Liu, G. B.; Feng, S. *J. Physica E* **2008**, *41*, 169–174. (c) Collins, J. B.; Levine, H. *Phys. Rev. B* **1985**, *31* (9), 6119–6122.
- (9) Choi, J. J.; Yang, X.; Norman, Z. M.; Billinge, S. J. L.; Owen, J. S. *Nano Lett.* **2014**, *14*, 127–133.

- (10) Poglitsch, A.; Weber, D. *J. Chem. Phys.* **1987**, *87* (11), 6373–6378.
- (11) Kitazawa, N.; Watanabe, Y.; Nakamura, Y. *J. Mater. Sci.* **2002**, *37*, 3585–3587.
- (12) Mashiyama, H.; Kurihara, Y.; Azetsu, T. *J. Korean Phys. Soc.* **1998**, *32*, s156–s158.
- (13) Colella, S.; Mosconi, E.; Fedeli, P.; Listorti, A.; Gazza, F.; Orlandi, F.; Ferro, P.; Besagni, T.; Rizzo, A.; Calestani, G.; Gigli, G.; Angelis, F. D.; Mosca, R. *Chem. Mater.* **2013**, *25*, 4613–4618.
- (14) Mosconi, E.; Amat, A.; Nazeeruddin, M. K.; Grätzel, M.; Angelis, F. D. *J. Phys. Chem. C* **2013**, *117*, 13902–13913.